Time-Dependent Effects of Focal Retinal Ischemia on Axonal Cytoskeleton Proteins

Chandrakumar Balaratnasingam, William H. Morgan, Louise Bass, Min Kang, Stephen J. Cringle, and Dao-Yi Yu

Purpose. To examine the time-dependent effects of focal axonal ischemia on the retinal ganglion cell (RGC) cytoskeleton.

Methods. Eight pigs were used. Small retinal arteriolar branches were occluded by argon laser to induce focal ischemic insults that were maintained for a period of 6 hours or 1 hour. Treated and untreated retinal segments were dissected from the eye after euthanatization. Each retinal segment followed the longitudinal projection of RGC axons from peripheral retina to the optic disc. Antibodies to phosphorylated neurofilament heavy, phosphorylation-independent neurofilament heavy (NFH), neurofilament light, neurofilament medium, microtubule, and microtubule-associated proteins were used to study the axonal cytoskeleton. Glial fibrillary acidic protein and TUNEL staining were also used to examine astrocyte and apoptotic changes, respectively. Comparisons were made between treated and untreated retinal segments.

Results. Cytoskeleton protein changes occurred within ischemic regions and also within retinal tissue on the disc side and peripheral side of the ischemic regions. NFH and microtubule proteins were the earliest cytoskeleton subunits that underwent change. Changes to all cytoskeleton proteins, apart from NFH, occurred in a time-dependent manner within regions of ischemia. In the time points studied, cytoskeleton changes occurred in the absence of detectable astrocyte changes and RGC apoptosis.

Conclusions. An ischemic insult induces RGC cytoskeleton protein change, implying that the local environment plays an important role in modulating axonal structure and function. Cytoskeleton proteins are likely to be important pathogenic mediators of neuronal dysfunction in diseases such as glaucoma and retinal vascular disease. (*Invest Ophthalmol Vis Sci.* 2010;51:3019–3028) DOI:10.1167/iovs.09-4692

The cytoarchitecture of the human retinal ganglion cell (RGC) is elaborate and consists of a cell body that is connected to its target synapse by an axon that is approximately 1 μm in diameter and 50 mm in length.[1] The protracted course of the RGC axon makes it vulnerable to injury, and diseases modifying its structure remain a major cause of visual morbidity worldwide.[2] Cytoskeleton proteins are highly concentrated within the intracellular compartment of RGCs and are critical for stabilizing its complex axonal arborizations.[3,4] In addition to playing a structural role, cytoskeleton proteins regulate RGC axonal function through their involvement in vital homeostatic processes such as axonal transport, cell signaling, and synaptic plasticity.[5,6] Axonal injury results in acute cytoskeleton protein modification with the magnitude and temporal sequence of protein subunit dysfunction being intimately related to the form of axonal insult.[7–9] Neuronal fate after axonal injury is also known to be influenced by the cytoskeleton response, with the overexpression and underexpression of specific cytoskeleton protein subunits being important determinants of neuronal survival and death.[10] Because cytoskeleton proteins are inherently linked to neuronal function and survival, an understanding of the cytoskeleton protein response after various modes of RGC axonal injury may provide important information about the pathogenic mechanisms responsible for RGC death in different ocular diseases.

Glaucoma is the second most common cause of blindness in the developed world,[11] and although it is generally agreed that the optic nerve head is a critical site for RGC axonal injury in this disease,[12] the pathogenic mechanisms underlying glaucomatous axonal loss and the resultant optic nerve head atrophy remains unresolved. The two major pathophysiological theories that have been proposed to explain the process of glaucomatous optic neuropathy are a mechanical, intraocular pressure–induced mechanism of axonal injury[13] and, a vascular, ischemia-induced mechanism.[14] However, recent studies have identified the presence of both mechanical and vascular processes, which function concurrently, during intraocular pressure (IOP)–induced RGC axonal degeneration, thereby providing evidence that mechanical and vascular mechanisms of glaucomatous optic neuropathy are not mutually exclusive.[15] We have performed detailed experiments that have examined the temporal sequence of change in astrocytes,[16] mitochondria,[17] and cytoskeleton proteins,[7,18] and effects on axonal transport,[7,18] apoptosis,[16] and nitric oxide synthase[19] systems within the optic nerve head after acute IOP elevation. As a result, we have demonstrated that an IOP-induced insult to the RGC axon results in dramatic cytoskeleton protein alteration that precedes disruption of other critical cellular processes. A similar study examining the sequence of cytoskeleton protein change after a purely ischemic insult to RGC axons has not been performed.

In vivo studies in our laboratory have measured oxygen consumption in different retinal layers.[20] The high concentration of mitochondria in the nerve fiber layer of the retina suggests that RGC axons are energy-intensive structures with a high basal rate of metabolism.[21] Dollery et al.,[22] Shakib and Ashton,[23] and McLeod et al.[24] examined the structural and functional consequences of retinal ischemia and demonstrated the vulnerability of RGC axons to injury during states of nutri-

From the Centre for Ophthalmology and Visual Science and the ARC Centre of Excellence in Vision Science, The University of Western Australia, Perth, Australia.

Supported by the National Health and Medical Research Council of Australia and the Australian Research Council Centre of Excellence in Vision Science.

Submitted for publication September 26, 2009; revised November 27 and December 20, 2009; accepted December 22, 2009.

Disclosure: **C. Balaratnasingam**, None; **W.H. Morgan**, None; **L. Bass**, None; **M. Kang**, None; **S.J. Cringle**, None; **D.-Y. Yu**, None

Corresponding author: Dao-Yi Yu, Centre for Ophthalmology and Visual Science and the ARC Centre of Excellence in Vision Science, The University of Western Australia, Perth, WA, Australia; dyyu@cyllene.uwa.edu.au.

ent deprivation. These studies identified significant intra-axonal structural disruption in the form of vacuolation[22,23] and intra-axonal functional disruption in the form of axonal transport retardation[24] after a brief period of regional retinal ischemia. In these studies, a pig eye model of focal retinal ischemia was used, with the results of the latter study demonstrating that retinal cotton wool spots are a consequence of inhibition of regional RGC axonal transport.[24]

Although these studies have greatly increased our knowledge about the pathogenic processes underlying neuronal dysfunction in retinal vascular disease, they have not provided us with an in-depth understanding of axonal cytoskeleton behavior during states of retinal ischemia. Each cytoskeleton protein subunit serves a unique purpose within neuronal cells, and an understanding of cytoskeleton protein subunit modification in ischemia may identify key cellular changes that are important in the development of neuronal death and irreversible axonal injury. Furthermore, because the axonal cytoskeleton regulates neuronal function[5] and is in continuous communication with retinal astrocytes,[25] a detailed understanding of neuronal cytoskeleton change in ischemia may aid in the pathophysiological understanding of axonal transport and axonal structural changes that have been reported in experimental ischemic studies.

In this study, we used a well-established pig model of focal retinal ischemia to examine the temporal sequence of change to neurofilament subunits, microtubules, and microtubule-associated proteins (MAPs) within RGC axons. Markers for apoptosis and astrocytes are also used to determine whether cell death and glial alteration are precursors of cytoskeleton change after an ischemic insult. We also investigated cytoskeleton and astrocyte changes on the disc and peripheral sides of ischemic regions, to determine whether cytoskeleton and astrocyte changes occur outside the region of ischemia. Finally, we compared the results of cytoskeleton protein change after an ischemia-induced insult to the RGC axon with our previous results of IOP-induced insults to the RGC axon.[7,18] To improve our knowledge about pathogenic mechanisms leading to axonal degeneration in glaucoma and retinal ischemia we correlated the chronology of cytoskeleton protein change in this study with previous reports that have documented the structural and functional effects of retinal ischemia on RGC axons.[22–24]

Materials and Methods

General

Eight female White Landrace pigs, aged 8 to 11 weeks and weighing between 18 and 31 kg were used. Food was withheld for 12 hours and water for 0.5 hours before each experiment. All experiments were conducted and all laboratory animals treated in accordance with the ARVO Statement for the Use of Animals in Ophthalmic and Vision Research. The study was approved by the University of Western Australia Animal Ethics Committee. Four pig eyes were also obtained from the local abattoir and used for studying normal retinal astrocyte distribution.

Anesthesia

Anesthesia was induced with an intramuscular injection of tiletamine/zolazepam 4.4 mg/kg (Zoletil 100 mg/mL; Virbac, Peakhurst, NSW, Australia) and xylazine 2.2 mg/kg (Xylazil 100 mg/mL; Troy Laboratories, Smithfield, NSW, Australia). Anesthesia was maintained with a constant-rate infusion of propofol 12 mg/kg/h (Fresol 1%; Fresenius Kabi Austria GmbH, Graz Austria) and a constant-rate infusion of fentanyl citrate 30 μg/kg/h (fentanyl injection 50 μg/mL; Mayne Pharma Pty. Ltd., Mulgrave, VIC, Australia). Pancuronium (pancuronium injection BP 2 mg/mL; AstraZeneca, North Ryde, NSW, Australia) was given at 0.2 mg/kg IV followed by a constant-rate infusion of 0.3 mg/kg/h IV to induce muscle relaxation.

After induction, pigs were placed in sternal recumbency, intubated, and ventilated (Ohmeda 7000; BOC Health Care, Madison, WI). Ventilator settings were adjusted to maintain end-tidal carbon dioxide ($PaCO_2$) tensions between 30 and 45 mm Hg. Oxygen and nitrogen flow rates were adjusted to maintain arterial oxygen tensions between 80 and 100 mm Hg. Inspired oxygen concentrations and end-tidal carbon dioxide tensions were monitored continuously (Capnomac Ultima; Datex, Helsinki, Finland). The auricular artery was catheterized for continuous blood pressure measurement (Gould P23 ID pressure transducers connected to a conditioning module; Analog Devices, Norwood, MA) and to allow collection of arterial blood samples. Arterial blood gas samples were collected every 60 minutes to permit measurement of pH, carbon dioxide, and oxygen tensions (model 238 pH/blood gas analyzer; CIBA Corning Diagnostics, Halsted, UK). Heart rate was monitored via electrocardiogram (Cardiocap; Datex).

Diastolic pressure was maintained above 60 mm Hg by administering a balanced isotonic fluid solution (Hartmann's, Baxter Health Care Pty. Ltd., Toongabbie, NSW, Australia) at 10 mL/kg/h, supplemented when necessary with dobutamine 1 to 5 μg/kg/h (dobutamine injection 12.5 mg/m; Mayne Pharma Pty. Ltd., Mulgrave VIC, Australia) and/or dextran 70 at 5 to 10 mL/kg/h (Gentran 70 6% wt/vol; Baxter Health Care Ltd., Thetford, UK). Intravenous fluids and drugs were administered via a 22-gauge, 1-in. catheter (Insyte; BD Medical Systems, Inc., Sandy, UT) in the auricular vein.

Rectal temperature was maintained between 37°C and 39.5°C with a thermal blanket (Homeothermic Blanket Control Unit; Harvard Apparatus, Ltd., Edenbridge, UK) beneath and atop the pig. Plastic bubble wrap was used at the extremities to reduce heat loss. Euthanatization on completion of the experiment was achieved with an anesthetic overdose of intravenous pentobarbitone sodium 160 mg/kg (300 mg/mL, Lethabarb; Virbac Pty. Ltd., Peakhurst, NSW, Australia).

Focal Retinal Ischemia Model

Focal retinal ischemic lesions were induced by occlusion of a small branch of second- or third-order arterioles with previously reported photochemical thrombosis techniques.[26] Both eyes of each animal were treated. In this study, we induced two retinal ischemic lesions per eye: (1) The first lesion was induced at the beginning of the experiment and remained ischemic for 6 hours. (2) The second lesion was induced at a different retinal location 5 hours after the first set and remained ischemic for only 1 hour.

Tropicamide 1% and phenylephrine 10% were instilled topically at the beginning of each experiment to induce pupil dilation. Baseline fundus photographs and fluorescein angiography images of each eye were then captured with fluorescein angiography and a retinal camera (TRC-50VT; Topcon Medical Systems, Inc., Paramus, NJ). Sodium fluorescein 10% at a dose of 1 mL/10 kg (PharmaLab, Sydney, NSW, Australia) was injected through the auricular vein for fluorescein angiogram studies.

After baseline fundus photography, the retinal arterioles were occluded by laser photocoagulation. Our technique of photocoagulation consisted of an intravenous injection of rose bengal (Sigma-Aldrich, Castle Hill, NSW, Australia), at a dose of 10 mg/kg, after which retinal arterioles were treated with argon green laser (532 nm; Iris Medical Instruments, Inc., Mountain View, CA) using a slit lamp delivery system (SL-980; CSO, Firenze, Italy) and a corneal contact lens (Goldmann 902S 1-mirror lens; Haag-Streit, Bern, Switzerland). Laser parameters included a spot size of 75 μm, exposure time of 1000 ms, and power of 190 mW. Between 10 and 15 laser spots were necessary to induce complete occlusion of each arteriole. Color fundus and fluorescein angiogram photos were acquired immediately after laser treatment to confirm total vessel occlusion (Figs. 1A, 1B). For the first set of retinal lesions, fundus and fluorescein images were also collected 5 and 6 hours after vessel occlusion. For the second set of retinal lesions a series of images were obtained 1 hour after vessel occlusion. Histologic

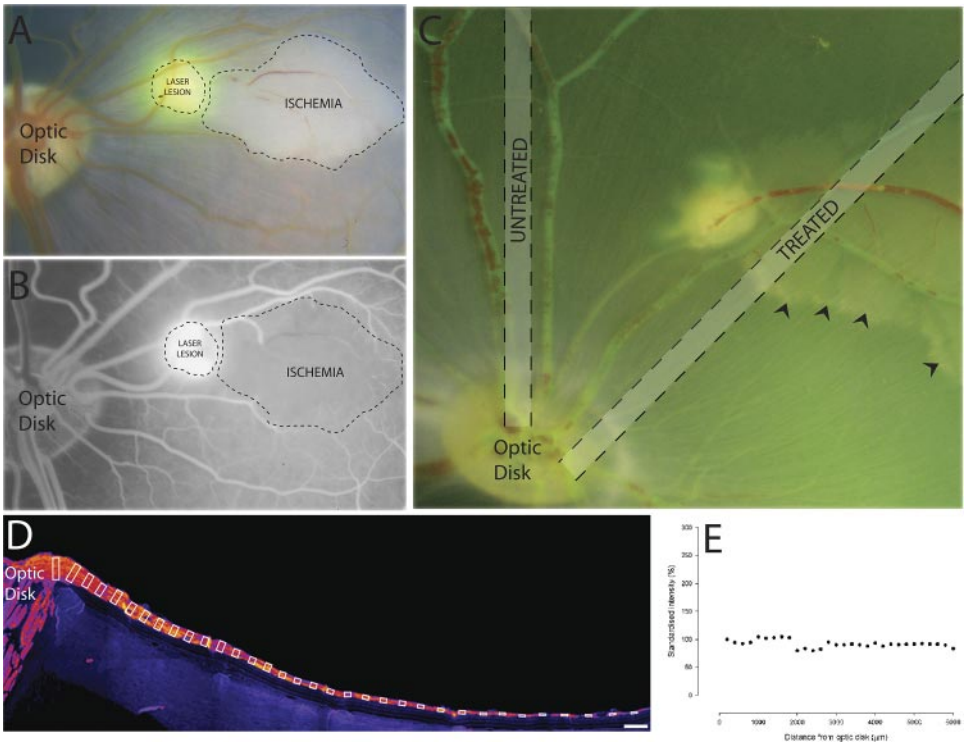

FIGURE 1. Experimental arteriolar occlusion and image analysis. A color fundus photograph (**A**) and corresponding fluorescein angiogram image (**B**) illustrate the pale discoloration and nonperfusion of ischemic regions after laser-induced arteriolar occlusion. Images collected with the dissecting microscope (**C**) demonstrate the gross morphology of untreated and treated segments that were dissected with a straight blade (*fenestrated line*). After 6 hours of ischemia, prominent swelling in the boundary zone between ischemic and nonischemic retina (*arrowheads*) was present in some specimens. Digital images of antibody-labeled slides (**D**) were quantified by determining the mean pixel intensity of the NeFL, at 200-μm intervals, commencing at the optic disc and extending to the peripheral retina. The dimensions of the ROI at each point of sampling corresponded to the thickness of the NeFL at that location (**D**, *white boxes*). (**E**) Raw values were standardized and are expressed as a percentage of the of the pixel intensity of the first point that was sampled. Scale bar, 300 μm.

analysis was performed only on those retinal lesions that had remained occluded and ischemic for the desired period. Lesions that demonstrated evidence of reperfusion were excluded from the study.

Tissue Preparation

Eyes, together with their optic nerves, were immediately enucleated after euthanatization. After a 5-mm pars plana incision, each globe was immersed in 4% paraformaldehyde solution for 2 hours. The anterior segment and vitreous were then removed before the remaining eye cup was immersed in a fresh solution of 4% paraformaldehyde for another 4 hours. After fixation, guided by a dissecting microscope, we used a straight blade to divide the retina into segments (Fig. 1C). All segments commenced at the optic disc and extended into the peripheral retina. Stringent measures were adopted for dissection to ensure that the boundary of each segment was aligned parallel to the direction of the axonal fibers. Color photographs, fluorescein angiograms, and fundus drawings were correlated with the macroscopic tissue appearance to identify regions of retinal ischemia before dissection. Dissected retinal segments were divided into two groups (Fig. 1C): untreated segments that were devoid of ischemia and laser lesions and treated segments that had no laser lesions. The treated segments consisted of a region of retinal ischemia with associated retinal tissue on the disc and peripheral sides of the ischemic region. They were divided into 1-hour and 6-hour groups. From each eye, we used only one section for each time point.

After microscopic dissection, individual retinal segments were cryoprotected by immersion in 30% sucrose overnight at 4°C. The segments were then embedded in optimal cutting temperature compound (Tissue-Tek 4583, product no. 62550-12; Sakura Finetec, Tokyo, Japan) and sectioned at 12 μm on a cryotome set at −30°C. Before sectioning, the segments were aligned such that the direction of axons in the nerve fiber layer ran parallel to the blade on the cryotome. The sections were subsequently used for immunohistochemical and TUNEL staining.

Immunohistochemistry

Sections from all segments were used for cytoskeleton antibody staining. For astrocyte antibody staining, only sections from the untreated and 6-hour–treated groups were used. Flat-mounted retinal specimens from four pig eyes obtained from the local abattoir were also used for astrocyte antibody staining.

All primary antibodies were made into solution with 1% goat serum (G9023; Sigma-Aldrich) and 1% bovine serum albumin. Triton X-100 (0.1%; Sigma-Aldrich) was also used for all primary antibody incubations to improve permeability. The primary antibodies used in the study of the cytoskeleton were polyclonal antibody NF-L, directed against the neurofilament light subunit (1:500, AHP286; Serotec, Oxford, UK); monoclonal antibody NF-M, directed against the neurofilament medium subunit (1:200, N5264, Clone NN18; Sigma-Aldrich); monoclonal antibody NF-H, directed against the phosphorylated and nonphosphorylated neurofilament heavy subunit (1:400, N0142, Clone N52; Sigma-Aldrich); monoclonal antibody NF-Hp, directed against the phosphorylated neurofilament heavy subunit (1:200, N5389, clone NE14; Sigma-Aldrich); monoclonal antibody Tub, directed against isotypes I and II of β-Tubulin (1:200, T8535, Clone JDR.3B8, Sigma-Aldrich); and anti MAP-1 antibody (1:200, M4278; Sigma-Aldrich). We used a mouse monoclonal antibody to GFAP derived from porcine immunogen as an astrocyte marker (1:500, G3893, Clone G-A-5; Sigma-Aldrich). After primary antibody incubation, the slides were washed and then incubated with either a goat anti-mouse IgG (1:400; Alexa Fluor 488, A11001; Molecular Probes, Portland, OR) or a goat anti-rabbit IgG (1:400; Alexa Fluor 488, A11008; Molecular Probes, Portland, OR) secondary antibody. After incubation, the sections were washed and mounted in glycerol before study under a confocal microscope.

Apoptosis Detection with TUNEL Staining

Sections from the untreated and 6-hour–treated segments were used for TUNEL staining. Recombinant terminal transferase (Roche Pharmaceuticals, Sydney, NSW, Australia) and biotin16-dUTP (Roche Pharmaceuticals) labeled with fluorescein avidin D (Vector Laboratories, East Brisbane, QLD, Australia) were used to identify DNA fragmentation. Tissues were fixed in 4% paraformaldehyde for 20 minutes, rinsed, and incubated in permeabilization solution (0.1% Triton X-100 in 0.1% sodium citrate) for 2 minutes on ice. After the section were rinsed, the TUNEL reaction mixture was applied to the slides, which were then

TABLE 1. Physiological Data for Individual Pigs

Pig	HR	BP	PaO_2	$PaCO_2$	RR	pH
1	105.3 ± 8.6	90 ± 2.9	126.5 ± 3.4	40.5 ± 1.7	14.5 ± 0.1	7.5 ± 0.0
2	102.5 ± 2.1	105.8 ± 2.2	103.7 ± 4.2	41.4 ± 1.5	14.1 ± 0.1	7.5 ± 0.0
3	92.0 ± 2.5	97.4 ± 1.2	113.3 ± 2.1	34.2 ± 1.8	14.1 ± 0.1	7.5 ± 0.0
4	99.9 ± 2.7	106.9 ± 2.2	105.8 ± 5.0	43.5 ± 0.6	14.0 ± 0.1	7.5 ± 0.0
5	84.3 ± 1.3	103.9 ± 1.9	101.4 ± 2.1	43.4 ± 1.3	13.0 ± 0.0	7.5 ± 0.0
6	82.3 ± 1.8	111.1 ± 1.3	108.1 ± 3.9	40.2 ± 1.0	12.0 ± 0.0	7.5 ± 0.0
7	113.4 ± 4.1	105.7 ± 3.6	106.5 ± 9.7	44.5 ± 2.6	14.2 ± 0.2	7.5 ± 0.0
8	121.6 ± 32	98.5 ± 1.0	108.9 ± 2.5	38.9 ± 0.8	14.0 ± 0.0	7.5 ± 0.0

coverslipped and incubated at 37°C for 120 minutes. These sections were then rinsed again and incubated in 1:50 fluorescein avidin D in PBS for 60 minutes. After this, the sections were rinsed a final time in 0.01 M PBS, dried, and mounted before visualization under the confocal microscope. Untreated segments that were incubated with DNase I, recombinant grade I (Roche) for 10 minutes at room temperature before application of the TUNEL reaction mixture were used as the positive control.

Microscopy

Low-magnification images of experimental lesions were obtained before retinal dissection by using a high-resolution digital camera (DP11; Olympus, Tokyo, Japan) attached to a dissecting microscope (SZ-STS; Olympus). Digital images of antibody and TUNEL-labeled sections were captured with a confocal laser scanning microscope (MRC 1000/1024 UV; Bio-Rad, Regents Park, NSW, Australia) controlled by image-acquisition software (COMOS; Bio-Rad). Visualization of all sections was achieved by laser excitation by a 488-nm line from an argon laser with emissions detected through a 522/535-nm band pass filter. Lenses used to view retinal sections included a Plan 10× (NA 0.3; Nikon, Tokyo, Japan), Plan 40× (NA 0.7; Nikon), and Plan-Apo 20× (NA 0.75; Nikon) dry lens.

With a motorized stage and the use of a macro (written in MPL under COMOS; Bio-Rad), a series of Z stacks were captured for each slide, beginning in the optic nerve head and extending approximately 8 mm into the peripheral retina. The images were collected in gray scale (on a scale of 0–255). Each Z stack comprised a depth of optical sections collected at 2-μm increments along the z-plane. Each contained seven sequential images that were collected by using Kalman averaging. The stacks were then montaged by using a plugin in Image J (version 1.36, developed by Wayne Rasband, National Institutes of Health, Bethesda, MD; available at http://rsb.info.nih.gov/ij/index.html). Creating a montage allowed us to study spatial changes in cytoskeleton protein and astrocyte and TUNEL staining between the optic disc and peripheral retina. The average projection of each montaged Z stack was used for quantitative analysis.

Image Analysis

Quantitative image analysis was performed (Image Pro Plus, ver. 5.1; Media Cybernetics, Bethesda, MD), and the images were prepared for the article (Photoshop CS2 and Adobe Illustrator CS2, ver. 12.0; Adobe Systems Inc., San Jose, CA). Confocal images were pseudocolored using the Look Up Tables feature of Image J. In this study, we performed quantitative analysis only of the retinal nerve fiber layer. Sections labeled with cytoskeleton and astrocyte antibodies were quantified as follows (Figs. 1D, 1E):

1. For each image, the point of intersection between the optic disc and retina was used as a reference point (0 μm) for distance.
2. The mean pixel intensity of the nerve fiber layer was determined at 200-μm intervals, commencing at the optic disc and extending into the peripheral retina. The dimension of the region of interest (ROI) used for pixel intensity measurements was adjusted so that it corresponded with the thickness of the nerve fiber layer at the point of sampling (Fig. 1D). This method of quantification allowed us to account for the change in axon number and nerve fiber layer thickness across the retina in untreated tissue. It also allowed us to account for changes in nerve fiber layer thickness due to retinal edema in treated tissue. The nerve fiber layer was quantified from the reference point to approximately 8 mm into the peripheral retina.
3. Mean pixel intensity within each ROI was normalized and expressed as a percentage of the pixel intensity of the ROI closest to the optic disc (Fig. 1E).

Normalized pixel intensities were used for all statistical analyses.

Statistical Analysis

Kolmogorov-Smirnov testing was performed on all data before analysis, to determine whether data were normally distributed. Normally distributed data were analyzed by ANOVA with post hoc factor comparison performed with a paired Student's t-test with Bonferroni correction. Non-normally distributed data were analyzed using ANOVA on ranks, with the Tukey test used for post hoc paired analysis. Results are expressed as the mean ± SE (SigmaStat, ver. 3.1; SPSS, Chicago, IL).

We determined whether treated segments were significantly different from untreated segments by performing the following calculations before statistical analysis. First, regions of axonal ischemia in treated tissue were paired with points on untreated tissue that were an identical distance from the optic disc. The mean intensity of these points in treated and untreated tissue was determined.

Second, points on the disc and peripheral sides of the ischemic regions were paired with points on untreated tissue that were an identical distance from the optic disc. Only points within 2 mm of the ischemic boundary on the disc side and peripheral side of the ischemic regions were paired for analysis. The mean intensity of the disc- and peripheral-side regions within treated and untreated tissue was then determined.

Three-way ANOVA was used to assess the effects of the number of subjects, insult (untreated and treated), and location (disc side, ischemia, and peripheral side) on the parameter mean of the normalized pixel intensity.

RESULTS

Animal Physiology

The mean systolic blood pressure for all eight pigs was 102.4 ± 2.3 mm Hg. Blood gas analysis showed that average arterial pO_2 was 109.3 ± 2.8 mm Hg, pCO_2 was 40.8 ± 1.2 mm Hg, and pH was 7.5 ± 0.0. Mean heart rate was 100.1 ± 4.8 beats per minute and mean respiratory rate was 13.8 ± 0.3 breaths per minute. Mean experimental data for the individual pigs are presented in Table 1.

Retinal Changes after Laser-Induced Arteriolar Occlusion

Within minutes of arteriolar occlusion, there was gray discoloration of ischemic segments (Fig. 1A). These regions of gray discoloration corresponded very closely to angiographic re-

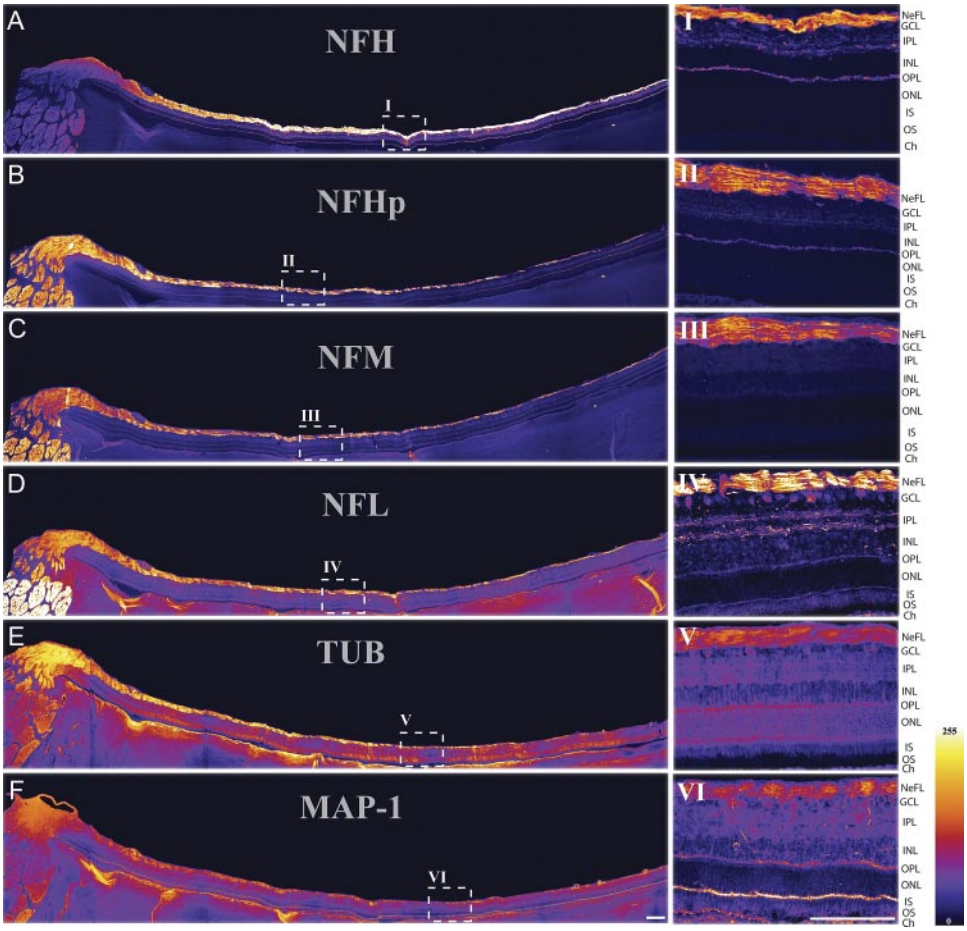

FIGURE 2. Cytoskeleton protein distribution in normal, untreated pig retina. Confocal microscope montages illustrate the distribution of NFH (**A**), NFHp (**B**), NFM (**C**), NFL (**D**), TUB (**E**), and MAP-1 (**F**) from peripheral retina to optic disc. (**I–VI**) High-magnification images of the distribution of these proteins within the different layers of the retina. Ch, choroid. *Bottom right*: color intensity scale. Scale bar, 200 μm.

gions of nonperfusion (Fig. 1B). There was no fluorescein leakage within the ischemic segments. After 6 hours of retinal ischemia, we observed increasing white discoloration on the disc side of some ischemic segments (Fig. 1C). This effect was most evident at the boundary zone between the ischemic and nonischemic regions and was similar in morphologic appearance to that described in previous reports of mitochondrial swelling and accumulation in the retina.[24]

Tissue Sections

Thirty-nine retinal segments were examined: 16 untreated and 23 treated. Of the 23 treated segments, there were 8 from the 1-hour group and 15 from the 6-hour group. Mean nerve fiber layer thickness within regions of ischemia in the 1-hour group was 128.3 ± 64.7 μm and in the 6-hour group was 198.2 ± 92.4 μm. Mean nerve fiber layer thickness in control sections at a distance from the optic disc as equivalent to that of the ischemic lesions was 88.7 ± 51.4 μm.

Distribution of Cytoskeleton Proteins in Normal, Untreated Pig Retina

Neurofilament Heavy (NFH). Staining for NFH was intense in the nerve fiber layer (NeFL) of the pig retina (Figs. 2A, 2AI). Less intense NFH staining was present in the ganglion cell layer (GCL), inner plexiform layer (IPL), and outer plexiform layer (OPL). We did not observe any NFH labeling in the inner nuclear layer (INL), outer nuclear layer (ONL), inner segment (IS) photoreceptor layer, or outer segment (OS) photoreceptor layer. In the NeFL, the intensity of axonal NFH staining was greater in the peripheral retina than that in the optic disc region ($P < 0.001$).

Phosphorylated Neurofilament Heavy (NFHp). There was very little NFHp antibody labeling in the GCL; however, staining was intense in the NeFL (Figs. 2B, 2BII). Weak staining for NFHp was also visible in the IPL and OPL. There was no difference in the intensity of NeFL NFHp staining in the optic disc and peripheral retinal regions ($P = 0.200$).

Neurofilament Medium (NFM). Staining for NFM was greatest in the NeFL of the pig retina (Figs. 2C, 2CIII). There was no difference in the intensity of NeFL NFM staining in the optic disc and peripheral retinal regions ($P = 0.415$).

Neurofilament Light (NFL). Staining for NFL was greatest in the NeFL (Figs. 2D, 2DIV). We also observed staining in the GCL, IPL, INL, OPL, IS, and OS of the pig retina. NFL stain was uniformly distributed along the course of the RGC axons in the NeFL, with no difference in the intensity of staining in the optic disc and peripheral retinal regions ($P = 0.085$).

Microtubule (TUB). Staining for microtubule protein was observed in all layers of the pig retina, apart from the OS (Figs. 2E, 2EV). The intensity of the staining was greatest in the NeFL. There was no difference in the intensity of NeFL TUB staining in the optic disc and peripheral retinal regions ($P = 0.082$).

Microtubule-Associated Protein (MAP)-1. Staining for MAP-1 was present in all layers of the pig retina (Figs. 2F, 2FVI). The intensity was greatest in the NeFL and IS and was only weakly present in the ONL. There was no difference in the intensity of NeFL MAP-1 staining in the optic disc and peripheral retinal regions ($P = 0.125$).

Comparison of Treated and Untreated RGC Axons

After 1 hour of ischemia, there was no difference in the intensity of staining for NFHp, NFM, NFL, and MAP-1 between

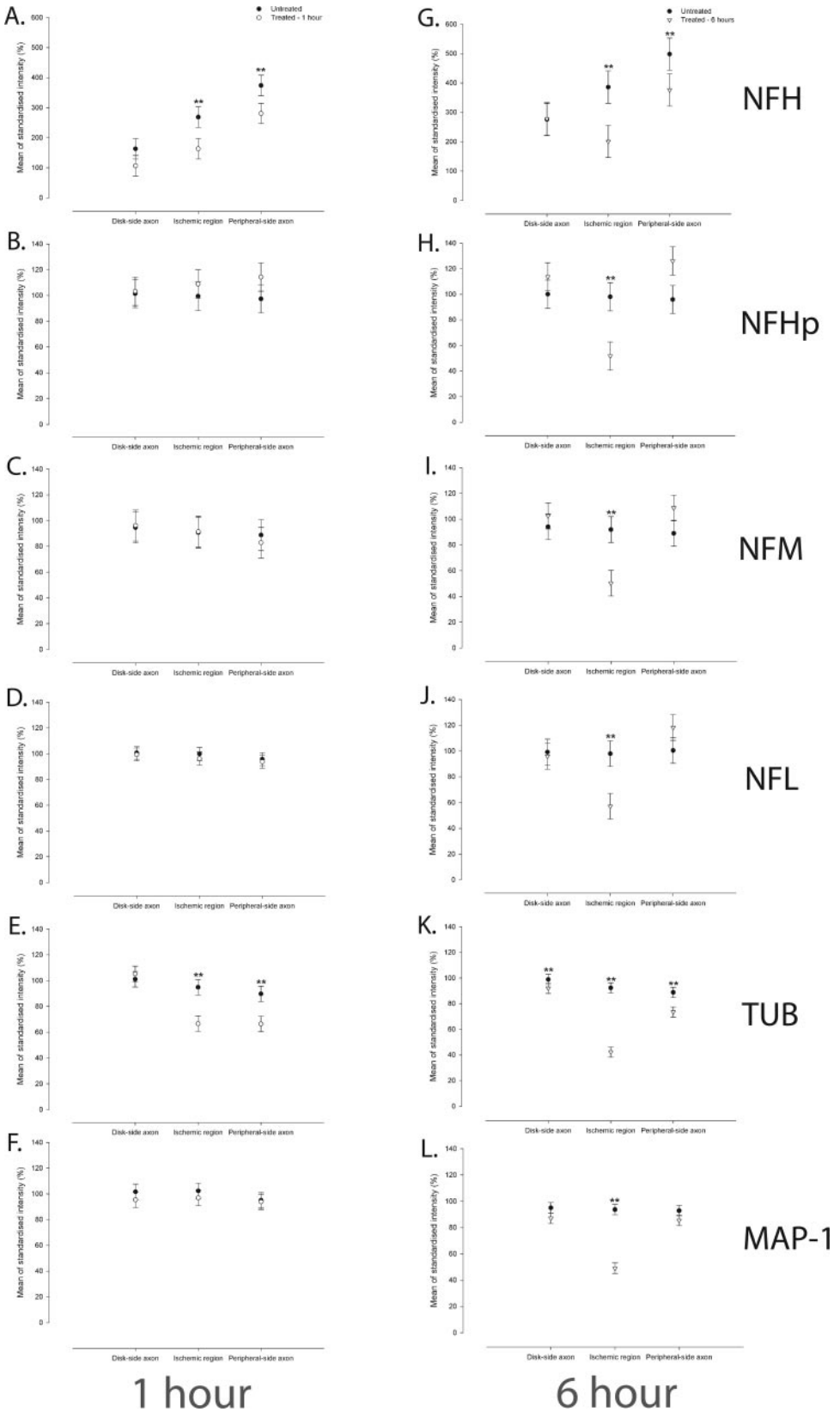

FIGURE 3. Quantitative analysis of changes in intensity of cytoskeleton protein staining after ischemia. Comparisons of staining intensities for NFH (**A**), NFHp (**B**), NFM (**C**), NFL (**D**), TUB (**E**), and MAP-1 (**F**) in untreated axons and treated axons that experienced 1 hour of ischemia demonstrated significant differences in TUB and NFH levels. Comparisons of staining for NFH (**G**), NFHp (**H**), NFM (**I**), NFL (**J**), TUB (**K**), and MAP-1 (**L**) in untreated axons and treated axons that experienced 6 hours of ischemia demonstrated significant differences in the levels of all cytoskeleton proteins. Mean staining intensities in disc- and peripheral-side axons were determined by pooling 10 ROI measurements in each of these regions. The mean for the ischemic region was determined by pooling all ROI measurements within this region. **Significant difference, as determined by ANOVA.

the treated and untreated axons (all $P > 0.569$; Fig. 3). There was a decrease in TUB and NFH within the regions of ischemia and on the peripheral side of the ischemic regions in treated axons ($P < 0.001$; Fig. 3). Post hoc analysis revealed that this decrease was significant in five of eight eyes.

After 6 hours of ischemia, there was a significant decrease in the intensity of staining for all cytoskeleton proteins in the ischemic region when compared with that in untreated axons (all $P < 0.033$; Figs. 3, 4). Post hoc analysis revealed that this decrease was significant in all animals. We observed a signifi-

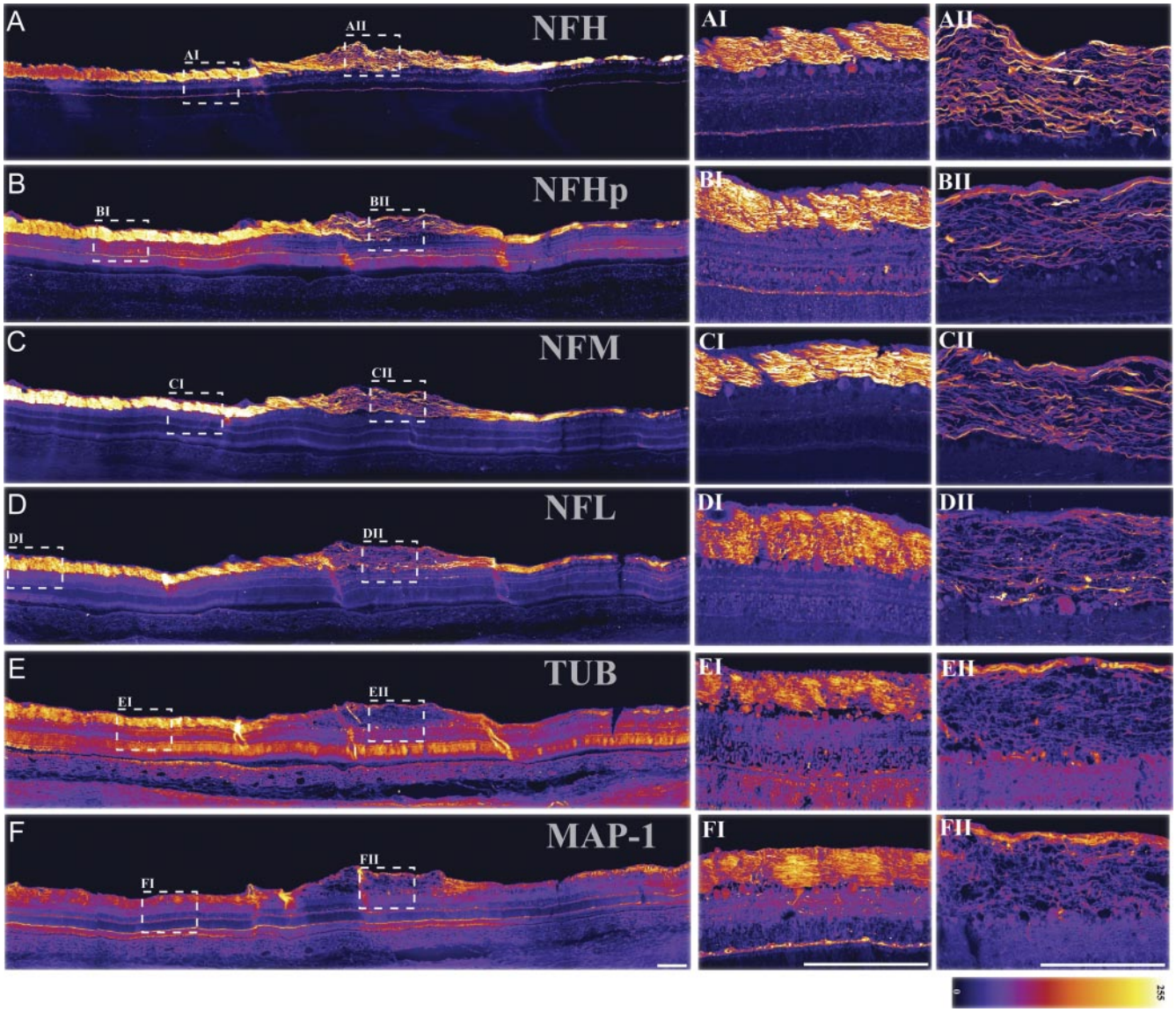

FIGURE 4. Changes in cytoskeleton protein levels 6 hours after retinal ischemia. Montaged confocal microscope images illustrate cytoskeleton protein expression in ischemic regions and within retinal tissue on the disc and peripheral sides of the ischemic regions. Specimens were stained for NFH (**A**), NFHp (**B**), NFM (**C**), NFL (**D**), TUB (**E**), and MAP-1 (**F**). (**I**, **II**) High-magnification comparisons of cytoskeleton protein staining on the disc side of the ischemic region and in the ischemic region, respectively, for each of the antibodies. All cytoskeleton proteins demonstrated an observable decrease in stain intensity in regions of ischemia. *Bottom right:* color intensity scale. Scale bar, 200 μm.

cant decrease in staining for TUB and MAP in the deeper layers of the NeFL, with very little change in the level of these proteins at the inner limiting membrane and vitreous border. NFH protein levels were also decreased on the peripheral side of the ischemic region ($P = 0.003$). In addition to that in the regions of ischemia, levels of TUB proteins were decreased on the disc and in peripheral sides of the ischemic region (both $P < 0.010$).

Time-Dependent Analysis of Cytoskeleton Change

Comparisons made between RGC axons exposed to 1 hour and 6 hours of regional ischemia showed a significant difference in cytoskeleton antibody intensity for all proteins, apart from NFH, in the region of ischemia (all $P < 0.049$). The intensity of cytoskeleton protein expression after 6 hours of ischemia was less than that in the 1-hour group. We did not find a significant time-dependent change in cytoskeleton protein intensity on the disc or the peripheral side of the ischemic region when the intensities at the two time points were compared (all $P > 0.104$).

GFAP Staining in the Normal Pig Retina and after Ischemia

Flat-mounted sections of normal retina demonstrated an elaborate network of GFAP-stained astrocyte processes in the retinal NeFL. GFAP staining was intense around the superficial retinal vasculature where dense astrocyte processes encircled the vessel profiles (Fig. 5A). Although dual labeling of axons and astrocytes was not performed, astrocytic processes formed distinct bundles in the NeFL that followed the direction of the RGC axons as they projected from the peripheral retina toward the optic disc (Fig. 5B). Analysis of retinal cross sections demonstrated a high intensity of GFAP stain in the NeFL. Less intensely stained GFAP-positive processes, most likely those of Müller cell inner processes and endfeet, were observed to

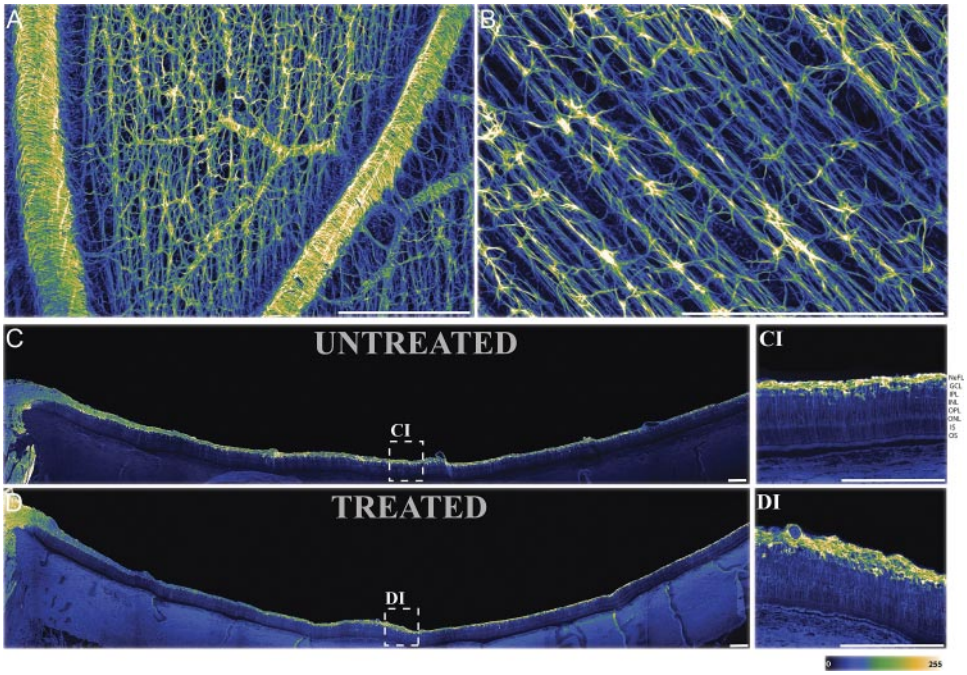

FIGURE 5. GFAP staining in untreated and treated pig retina. (**A**) Low- and (**B**) high-magnification images of flat-mounted normal, untreated pig retina demonstrate the dense network of astrocytic processes in the NeFL. These processes were most prominent around vascular structures and ran parallel to the direction of RGC axons. Confocal microscope montages illustrate the distribution of GFAP in untreated retina (**C**) and after 6 hours of retinal ischemia (**D**). (**CI**) High-magnification image of normal, untreated retina demonstrates the projection of Müller cell inner processes and end feet. (**DI**) There was no change in GFAP intensity in regions of ischemia despite the presence of NeFL swelling. Ch, choroid. *Bottom right:* color intensity scale. Scale bar, 200 μm.

extend from the inner limiting membrane to the outer retinal layers (Fig. 5CI). There was no difference in the intensity of NeFL GFAP staining in the optic disc and peripheral retinal regions ($P = 0.303$; Fig. 5C). In comparison to that in the untreated NeFL, the overall intensity of GFAP did not decrease significantly after 6 hours of ischemia ($P = 0.063$; Figs. 5D, DII). Post hoc analysis revealed that there was no difference in the intensity of stain within the regions of ischemia ($P = 0.345$).

TUNEL Stain

Positive control slides that were incubated with DNase before TUNEL labeling demonstrated numerous TUNEL-positive cells in the inner and outer nuclear layers of the retina (Fig. 6A). In these sections, positive TUNEL staining was also present in the NeFL (Fig. 6AI). There was no TUNEL labeling in untreated segments or in the NeFL of specimens that were subjected to 6 hours of ischemia (Figs. 6B, 6BI).

DISCUSSION

There were three major findings in this study: (1) Cytoskeleton protein subunits, apart from NFH, have uniform concentrations along the intraretinal pathway of RGC axons. (2) Focal retinal ischemia induces acute, time-dependent changes in cytoskeleton protein subunits that occur in the absence of detectable astrocyte changes and RGC apoptosis. (3) Localized RGC axonal ischemia causes selective cytoskeleton protein changes within retinal tissue on the disc side and peripheral side of regions of ischemia.

Cytoskeleton proteins are important determinants of neuronal architecture, and their pattern of distribution along axonal arborizations is an important cellular adaptation that permits the cell to cope with regional variations in metabolic stress and energy supply. The results of this study, combined with those in our previous report, highlight important differences between the intraretinal and optic nerve head portion of the RGC axon.[27] With the exception of the NFH, all cytoskeleton proteins examined in this study were uniformly distributed along the intraretinal pathway of the RGC axons. This observation contrasts significantly with that of the optic nerve head where there is a significant disparity in cytoskeleton protein concentrations in the prelaminar, lamina cribrosa, and postlaminar portions of the RGC axons.[27] Cytoskeleton protein expression is known to be influenced by myelin,[28] mitochondria,[29] and mechanical forces.[30] The presence of a significant

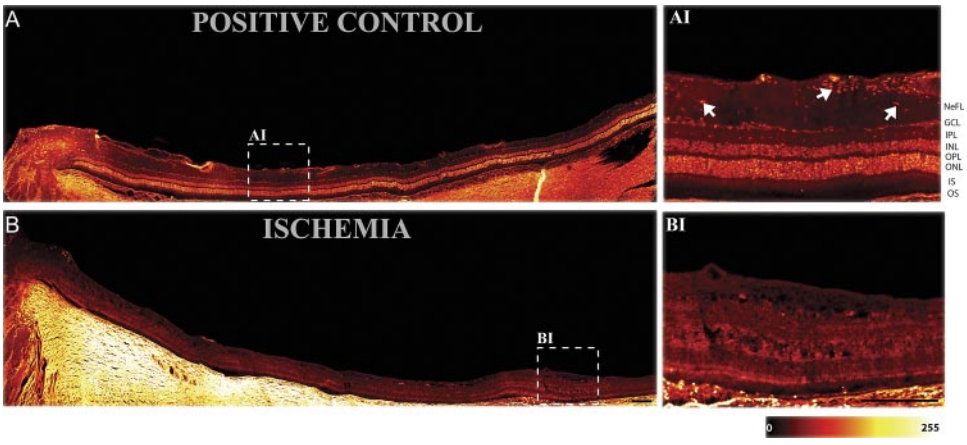

FIGURE 6. Confocal image montages illustrate the results of TUNEL staining in positive control slides (**A**) and after 6 hours of ischemia (**B**). (**AI**) High-magnification image of TUNEL-positive cells in the NeFL of positive control slides (*arrows*). (**BI**) Under high magnification, no TUNEL-positive cells were observed in the NeFL after 6 hours of ischemia. *Bottom right:* color intensity scale. Scale bar, 200 μm.

pressure gradient at the lamina cribrosa[31] and a reciprocal pattern of myelin and mitochondria distribution between post laminar and nonpostlaminar tissue[27] may explain some of the differences between optic nerve head and intraretinal portions of RGC axons. In this report, we cannot explain the reason for the decrease in NFH concentration in axonal tissue closer to the optic disc. Some studies have demonstrated an inverse relationship between axonal diameter and NFH concentration,[32] and the increase in RGC axonal diameter between cell soma and optic disc[33] may explain the corresponding decrease in NFH concentration between these two regions. It is also possible that the change in NFH concentration reflects the change in axon direction at the optic nerve head.

Because of inherent difficulties in the experimental induction of complete optic nerve head ischemia,[34] we used a laser-induced model of retinal arteriolar occlusion to study the effects of ischemic injury on the RGC axonal cytoskeleton. A major advantage in our experimental technique is that it allowed us to reliably induce and confirm vessel occlusion without disrupting optic nerve head structure through surgical manipulation. The mechanism of RGC axonal injury used in this study is different from that used in our previous experiments in which we examined the effects of IOP elevation[7,18] on the RGC cytoskeleton. In the present study, axonal changes were the consequence of a purely ischemic insult, whereas in previous experiments,[7,18] both vascular and mechanical components were involved in mediating axonal cytoskeleton changes. The present study demonstrates that an ischemic insult to the RGC axon causes an early cytoskeleton protein disruption within regions of ischemia. Similar to an IOP-induced insult,[7,16,18] the evolution of cytoskeleton protein change after ischemia occurs in a time-dependent manner in the absence of apoptotic changes. An important difference between an ischemic and IOP-induced insult on the RGC cytoskeleton is the sequence of protein subunit alteration. We have shown[7,18] that elevation of IOP results in early modification of all neurofilament protein subunits, with microtubule disruption occurring only after extended periods of IOP increase. This sequence of change in cytoskeleton proteins contrasts significantly with that occurring in ischemia where microtubules are affected before most neurofilament proteins. Cellular enzyme systems have strong influence over cytoskeleton protein structure,[35] and the order in which biochemical reactions are activated after injury may have some correlation with the sequence of alteration in cytoskeleton protein subunits. Previous experimental work has shown that elevation of IOP results in acute kinase enzyme activation,[36] whereas ischemia predominantly activates caspase enzyme systems during the early stages of injury.[37] The purpose of this study was not to identify the biochemical modulators of change in cytoskeleton protein levels; however, our results may provide the basis for understanding some of the histopathologic manifestations of ischemic axonal injury.[22–24] Cytoskeleton proteins are integral determinants of axonal architecture and also provide the scaffolding along which motor proteins travel during axonal transport.[38] Changes in cytoskeleton protein levels during ischemia may therefore underlie the development of intra-axonal structural changes such as vacuolation and intra-axonal functional changes such as axonal transport retardation. It is interesting that there was little observable change in TUB and MAP staining in the superficial layers of the NeFL after 6 hours of ischemia, despite a significant decrease in the intensity of change in the deeper layers of the NeFL. TUB and MAP subunits contribute to the cytoskeletal framework of glial cells[39,40] in addition to neurons, and the preservation of stain in the superficial layers of the NeFL, where glial processes are abundant, may reflect the heterogeneous nature of ischemia-mediated damage to neurons and glia.

By using montages of confocal microscope images, we were able to demonstrate that a focal ischemic insult to the RGC axon also induces selective change to NFH and microtubule proteins outside regions of ischemia. In this regard, the behavior of the RGC axon after ischemic injury is similar to other neurons in the central nervous system. Experimental work has demonstrated significant differences in neurofilament and microtubule–associated protein alteration between the ischemic core and perilesional nonischemic rim after focal cerebral ischemia.[41] Regional ischemia results in increased nitric oxide production in surrounding tissue,[42] and the resultant elevation in oxidative stress may account for some of the cellular changes in retinal tissue on the disc and peripheral sides of the ischemic regions. Alternatively, cytoskeleton protein alteration in regions on the disc and peripheral sides of ischemic tissue may be the consequence of neurotrophic deprivation secondary to axonal transport retardation within ischemic regions.[24]

The present study, in conjunction with our previous work,[7,18] demonstrates that change in cytoskeleton protein levels is an early marker of RGC axonal injury. It also implicates cytoskeleton protein subunits as important pathogenic mediators of neuronal dysfunction in diseases such as glaucoma and diabetic retinopathy. Because cytoskeleton proteins are rapidly altered after a range of neuronal insults, modalities that enable in vivo examination of the axonal cytoskeleton may have useful clinical applications for the identification of early neuronal injury in a variety of ocular diseases. The neuronal cytoskeleton is a major contributor of retinal NeFL birefringence,[43] and measures of birefringence by scanning laser polarimetry have already been used by investigators to identify and monitor RGC injury after optic nerve transection[44] and glaucoma.[45] The results in our present study suggest that measures of NeFL birefringence may also have utility for identifying threatened RGC populations in retinal vascular diseases such as diabetic retinopathy. In the present study we have not characterized the role played by individual cytoskeleton protein subunits in the process of axonal degeneration. This area is an important one that necessitates further work for clarification.

Acknowledgments

The authors thank Paul Rigby (The Centre for Microscopy, Characterization and Analysis, University of Western Australia) for help with the confocal scanning laser microscopy.

References

1. Mikelberg FS, Drance SM, Schulzer M, et al. The normal human optic nerve: axon count and axon diameter distribution. *Ophthalmology.* 1989;96:1325–1328.
2. Yong VK, Morgan WH, Cooper RL, et al. Trends in registered blindness and its causes over 19 years in Western Australia. *Ophthalmic Epidemiol.* 2006;13:35–42.
3. Fuchs E, Cleveland DW. A structural scaffolding of intermediate filaments in health and disease. *Science.* 1998;279:514–519.
4. Friede RL, Samorajski T. Axon caliber related to neurofilaments and microtubules in sciatic nerve fibers of rats and mice. *Anat Rec.* 1970;167:379–387.
5. Bray D, Gilbert D. Cytoskeletal elements in neurons. *Annu Rev Neurosci.* 1981;4:505–523.
6. Lariviere RC, Julien JP. Functions of intermediate filaments in neuronal development and disease. *J Neurobiol.* 2004;58:131–148.
7. Balaratnasingam C, Morgan WH, Bass L, et al. Time-dependent effects of elevated intraocular pressure on optic nerve head axonal transport and cytoskeleton proteins. *Invest Ophthalmol Vis Sci.* 2008;49:986–999.
8. Zhu B, Moore GR, Zwimpfer TJ, et al. Axonal cytoskeleton changes in experimental optic neuritis. *Brain Res.* 1999;824:204–217.

9. Serbest G, Burkhardt MF, Siman R, et al. Temporal profiles of cytoskeletal protein loss following traumatic axonal injury in mice. *Neurochem Res.* 2007;32:2006–2014.
10. Gotow T. Neurofilaments in health and disease. *Med Electron Microsc.* 2000;33:173–199.
11. Quigley HA. Number of people with glaucoma worldwide. *Br J Ophthalmol.* 1996;80:389–393.
12. Quigley HA. Ganglion cell death in glaucoma: pathology recapitulates ontogeny. *Aust N Z J Ophthalmol.* 1995;23:85–91.
13. Burgoyne CF, Downs JC, Bellezza AJ, et al. The optic nerve head as a biomechanical structure: a new paradigm for understanding the role of IOP-related stress and strain in the pathophysiology of glaucomatous optic nerve head damage. *Prog Retin Eye Res.* 2005; 24:39–73.
14. Yamamoto T, Kitazawa Y. Vascular pathogenesis of normal-tension glaucoma: a possible pathogenetic factor, other than intraocular pressure, of glaucomatous optic neuropathy. *Prog Retin Eye Res.* 1998;17:127–143.
15. Morgan JE. Optic nerve head structure in glaucoma: astrocytes as mediators of axonal damage. *Eye.* 2000;14:437–444.
16. Balaratnasingam C, Morgan WH, Bass L, et al. Elevated pressure induced astrocyte damage in the optic nerve. *Brain Res.* 2008; 1244:142–154.
17. Balaratnasingam C, Pham D, Morgan WH, et al. Mitochondrial cytochrome c oxidase expression in the central nervous system is elevated at sites of pressure gradient elevation but not absolute pressure increase. *J Neurosci Res.* 2009;87:2973–2982.
18. Balaratnasingam C, Morgan WH, Bass L, et al. Axonal transport and cytoskeletal changes in the laminar regions after elevated intraocular pressure. *Invest Ophthalmol Vis Sci.* 2007;48:3632–3644.
19. Balaratnasingam C, Ye L, Morgan WH, et al. Protective role of endothelial nitric oxide synthase following pressure-induced insult to the optic nerve. *Brain Res.* 2009;1263:155–164.
20. Yu DY, Cringle SJ. Oxygen distribution and consumption within the retina in vascularised and avascular retinas and in animal models of retinal disease. *Prog Retin Eye Res.* 2001;20:175–208.
21. Wang L, Dong J, Cull G, et al. Varicosities of intraretinal ganglion cell axons in human and nonhuman primates. *Invest Ophthalmol Vis Sci.* 2003;44:2–9.
22. Dollery CT, Henkind P, Paterson JW, et al. I. Ophthalmoscopic and circulatory changes in focal retinal ischaemia. *Br J Ophthalmol.* 1966;50:285–324.
23. Shakib M, Ashton N. II. Ultrastructural changes in focal retinal ischaemia. *Br J Ophthalmol.* 1966;50:325–384.
24. McLeod D, Marshall J, Kohner EM, Bird AC. The role of axoplasmic transport in the pathogenesis of retinal cotton-wool spots. *Br J Ophthalmol.* 1977;61:177–191.
25. Liuzzi FJ, Tedeschi B. Axo-glial interactions at the dorsal root transitional zone regulate neurofilament protein synthesis in axotomized sensory neurons. *J Neurosci.* 1992;12:4783–4792.
26. Danis RP, Bingaman DP, Yang Y, Ladd B. Inhibition of preretinal and optic nerve head neovascularization in pigs by intravitreal triamcinolone acetonide. *Ophthalmology.* 1996;103:2099–2104.
27. Balaratnasingam C, Morgan WH, Johnstone V, et al. Heterogeneous distribution of axonal cytoskeleton proteins in the human optic nerve. *Invest Ophthalmol Vis Sci.* 2009;50:2824–2838.
28. Dashiell SM, Tanner SL, Pant HC, Quarles RH. Myelin-associated glycoprotein modulates expression and phosphorylation of neuronal cytoskeletal elements and their associated kinases. *J Neurochem.* 2002;81:1263–1272.
29. Wagner OI, Lifshitz J, Janmey PA, et al. Mechanisms of mitochondria-neurofilament interactions. *J Neurosci.* 2003;23:9046–9058.
30. Price RL, Lasek RJ, Katz MJ. Internal axonal cytoarchitecture is shaped locally by external compressive forces. *Brain Res.* 1990; 530:205–214.
31. Morgan WH, Yu DY, Cooper RL, et al. The influence of cerebrospinal fluid pressure on the lamina cribrosa tissue pressure gradient. *Invest Ophthalmol Vis Sci.* 1995;36:1163–1172.
32. Xu Z, Marszalek JR, Lee MK, et al. Subunit composition of neurofilaments specifies axonal diameter. *J Cell Biol.* 1996;133:1061–1069.
33. Fitzgibbon T, Funke K. Retinal ganglion cell axon diameter spectrum of the cat: mean axon diameter varies according to retinal position. *Vis Neurosci.* 1994;11:425–439.
34. Chauhan BC, LeVatte TL, Jollimore CA, et al. Model of endothelin-1-induced chronic optic neuropathy in rat. *Invest Ophthalmol Vis Sci.* 2004;45:144–152.
35. Shea TB, Zheng YL, Ortiz D, Pant HC. Cyclin-dependent kinase 5 increases perikaryal neurofilament phosphorylation and inhibits neurofilament axonal transport in response to oxidative stress. *J Neurosci Res.* 2004;76:795–800.
36. Huang Y, Cen LP, Luo JM, et al. Differential roles of phosphatidylinositol 3-kinase/akt pathway in retinal ganglion cell survival in rats with or without acute ocular hypertension. *Neuroscience.* 2008; 153:214–225.
37. Singh M, Savitz SI, Hoque R, et al. Cell-specific caspase expression by different neuronal phenotypes in transient retinal ischemia. *J Neurochem.* 2001;77:466–475.
38. Almenar-Queralt A, Goldstein LS. Linkers, packages and pathways: new concepts in axonal transport. *Curr Opin Neurobiol.* 2001;11: 550–557.
39. Papasozomenos SC, Binder LI. Microtubule-associated protein 2 (MAP2) is present in astrocytes of the optic nerve but absent from astrocytes of the optic tract. *J Neurosci.* 1986;6:1748–1756.
40. Saez R, Burgal M, Renau-Piqueras J, et al. Evolution of several cytoskeletal proteins of astrocytes in primary culture: effect of prenatal alcohol exposure. *Neurochem Res.* 1991;16:737–747.
41. Bidmon HJ, Jancsik V, Schleicher A, et al. Structural alterations and changes in cytoskeletal proteins and proteoglycans after focal cortical ischemia. *Neuroscience.* 1998;82:397–420.
42. Chao CC, Hu S, Sheng WS, et al. Cytokine-stimulated astrocytes damage human neurons via a nitric oxide mechanism. *Glia.* 1996; 16:276–284.
43. Huang XR, Knighton RW. Microtubules contribute to the birefringence of the retinal nerve fiber layer. *Invest Ophthalmol Vis Sci.* 2005;46:4588–4593.
44. Fortune B, Cull GA, Burgoyne CF. Relative course of retinal nerve fiber layer birefringence and thickness and retinal function changes after optic nerve transection. *Invest Ophthalmol Vis Sci.* 2008;49:4444–4452.
45. Mohammadi K, Bowd C, Weinreb RN, et al. Retinal nerve fiber layer thickness measurements with scanning laser polarimetry predict glaucomatous visual field loss. *Am J Ophthalmol.* 2004; 138:592–601.